AD-A085 580 SCIENCE APPLICATIONS INC EL SEGUNDO CALIF F/G 18/3
AIRBLAST EXPERIMENTS FOR THE M-X SPUR.(U)
DEC 78 J E CRAIG DNA001-77-C-0280
UNCLASSIFIED SAI-79-569-LA DNA-4721F NL

1 OF 1
AD A 085580

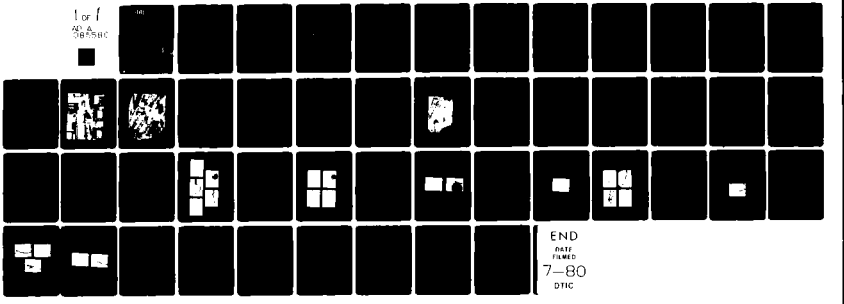

END
DATE FILMED
7-80
DTIC

LEVEL II

DNA 4721F

AIRBLAST EXPERIMENTS FOR THE M-X SPUR

Science Applications, Inc.
101 Continental Blvd, Suite 310
El Segundo, California 90245

31 December 1978

Final Report for Period 5 July 1977—31 December 1978

CONTRACT No. DNA 001-77-C-0280

THIS WORK SPONSORED BY THE DEFENSE NUCLEAR AGENCY
UNDER RDT&E RMSS CODE B344078464 Y99QAXSC35509 H2590D.

Prepared for
Director
DEFENSE NUCLEAR AGENCY
Washington, D. C. 20305

Destroy this report when it is no longer needed. Do not return to sender.

PLEASE NOTIFY THE DEFENSE NUCLEAR AGENCY, ATTN: STTI, WASHINGTON, D.C. 20305, IF YOUR ADDRESS IS INCORRECT, IF YOU WISH TO BE DELETED FROM THE DISTRIBUTION LIST, OR IF THE ADDRESSEE IS NO LONGER EMPLOYED BY YOUR ORGANIZATION.

UNCLASSIFIED

SECURITY CLASSIFICATION OF THIS PAGE (When Data Entered)

REPORT DOCUMENTATION PAGE		READ INSTRUCTIONS BEFORE COMPLETING FORM
1. REPORT NUMBER DNA 4721F	2. GOVT ACCESSION NO. AD-A085580	3. RECIPIENT'S CATALOG NUMBER
4. TITLE (and Subtitle) AIRBLAST EXPERIMENTS FOR THE M-X ~~SPUR~~		5. TYPE OF REPORT & PERIOD COVERED Final Report for Period 5 Jul 77—31 Dec 78
		6. PERFORMING ORG. REPORT NUMBER SAI-79-569-LA
7. AUTHOR(s) James E. Craig		8. CONTRACT OR GRANT NUMBER(s) DNA 001-77-C-0280
9. PERFORMING ORGANIZATION NAME AND ADDRESS Science Applications, Inc. 101 Continental Boulevard, Suite 310 El Segundo, California 90245		10. PROGRAM ELEMENT, PROJECT, TASK AREA & WORK UNIT NUMBERS Subtask Y99QAXSC355-09
11. CONTROLLING OFFICE NAME AND ADDRESS Director Defense Nuclear Agency Washington, D.C. 20305		12. REPORT DATE 31 December 1978 13. NUMBER OF PAGES 48
14. MONITORING AGENCY NAME & ADDRESS(if different from Controlling Office)		15. SECURITY CLASS (of this report) UNCLASSIFIED 15a. DECLASSIFICATION/DOWNGRADING SCHEDULE

16. DISTRIBUTION STATEMENT (of this Report)

Approved for public release; distribution unlimited.

17. DISTRIBUTION STATEMENT (of the abstract entered in Block 20, if different from Report)

18. SUPPLEMENTARY NOTES

This work sponsored by the Defense Nuclear Agency under RDT&E RMSS Code B344078464 Y99QAXSC35509 H2590D.

19. KEY WORDS (Continue on reverse side if necessary and identify by block number)

M-X Trench Spur
Airblast
Shock Propagation

20 ABSTRACT (Continue on reverse side if necessary and identify by block number)

A series of experiments was performed in the NASA Ames Electric Arc Shock Tube to investigate the propagation of strong shock waves (P ~ 40 BARS) in a model of the M-X Spur. The experiments were designed to measure incident and reflected shock pressures to provide a basis for the development of computer models for analysis of blast wave propagation in the M-X Spur. Since the M-X Spur is an asymmetric design, separate experiments were performed for flow by the Spur and flow into the Spur.

DD FORM 1 JAN 73 1473 EDITION OF 1 NOV 65 IS OBSOLETE

UNCLASSIFIED

SECURITY CLASSIFICATION OF THIS PAGE (When Data Entered)

20. ABSTRACT (Continued)

Initial and reflected shock pressures were recorded at several key locations in the model. The pressure loading on the model blast door was nonuniform along the door and was similar for loading from either direction. The maximum pressure on the blast door (P $\sim$ 80 BARS) occurred at the narrow portion of the Spur. The highest pressures in the model (P $\sim$ 130 BARS) occurred on the end of the turnout for flow into the Spur.

Two dimensional flowfield calculations were performed by TRW and Systems, Science and Software for flowfields related to the present tests. Favorable comparisons with measurements were obtained for flow by the Spur. Calculations for flow into the Spur did not compare well with the test data demonstrating the effect of late time flows for this orientation.

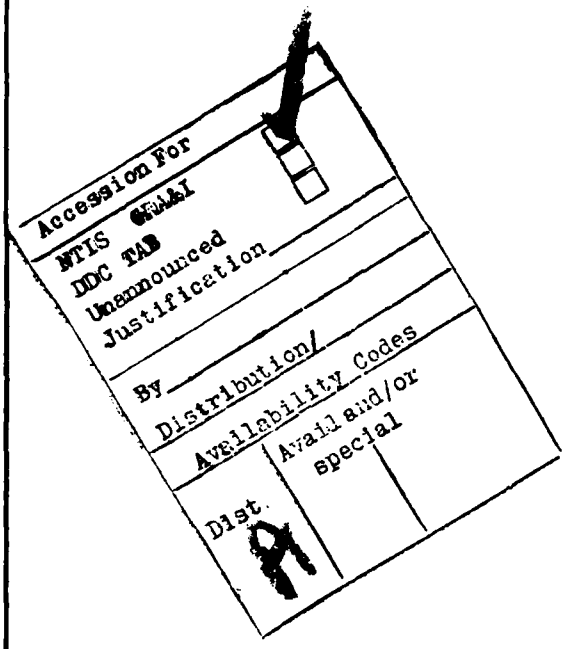

PREFACE

This program was conducted for the Defense Nuclear Agency under contract DNA001-77-C-0280 to provide experimental data on shock propagation in the M-X Spur. The effort was sponsored by the Strategic Structures Division of the Shock Physics Directorate and was performed during the period 1 March 1978 to 31 December 1978. Dr. George Ullrich was the DNA Technical Representative.

The SAI Program Manager was Duane Hove. Dr. James Craig conducted the shock tube tests and performed the data analysis.

We are grateful to Dr. Robert Dannenberg of the NASA Ames Research Center for continuing cooperation and suggestions.

TABLE OF CONTENTS

LIST OF FIGURES

LIST OF FIGURES (Con't)

LIST OF TABLES

NOMENCLATURE

A	Sound speed
C_S	Shock velocity
D	Tube diameter
E	Energy
m	Molecular weight
M	Mach number
P	Pressure
T	Temperature
U	Velocity
V	Volume
X	Distance
γ	Ratio of specific heats
Γ	Acoustic impedance
ρ	Fluid density

Subscripts

i	Initial
s	Shock
1,2,3,4	Shock tube region defined in Figure 9.

1.0 INTRODUCTION

An alternative to the M-X Trench with in-line Missile carriers is the spur concept in which missile carriers are stationed in off-line turnouts hardened against airblast loads. The two distinct differences between in-line and off-line missile basing are: 1) for the in-line concept the missile carrier can be stationed at any point in the trench whereas for the off-line concept the missile carrier can only be stationed in a finite number of locations, and 2) for the in-line concept the blast plug must survive a normal reflection of the airblast whereas for the off-line concept the blast plug loading is considerably reduced.

Two variations of the off-line basing concept are the single and double spurs (Figure 1). For the single spur concept, the missile carrier is based in the turnout which is protected from airblasts in the trench by a blast plug. For the double spur concept the missile carrier uses the turnout to maneuver into the double spur located across the trench. The blast plug for the double spur is aligned with the trench whereas for the single spur the blast plug is at a 60^0 to the trench axis.

The asymmetric geometry of the spur concept causes the blast door loading to depend upon direction of loading. Accurate vulnerability assessments of the spur concept require experimental and calculational programs. Experiments have been performed in the NASA/Ames Research Center Electric Arc Shock Tube in which the airblast environment was recorded in a 1:33 scale model of a double spur. The experiments used an incident shock pressure ratio of 40 (300 psi in air at ½ atmosphere) to determine the shock propagation in the spur. Tests were conducted from both orientations. Pressure histories were obtained from high frequency transducers located on the blast door and at selected points through the model.

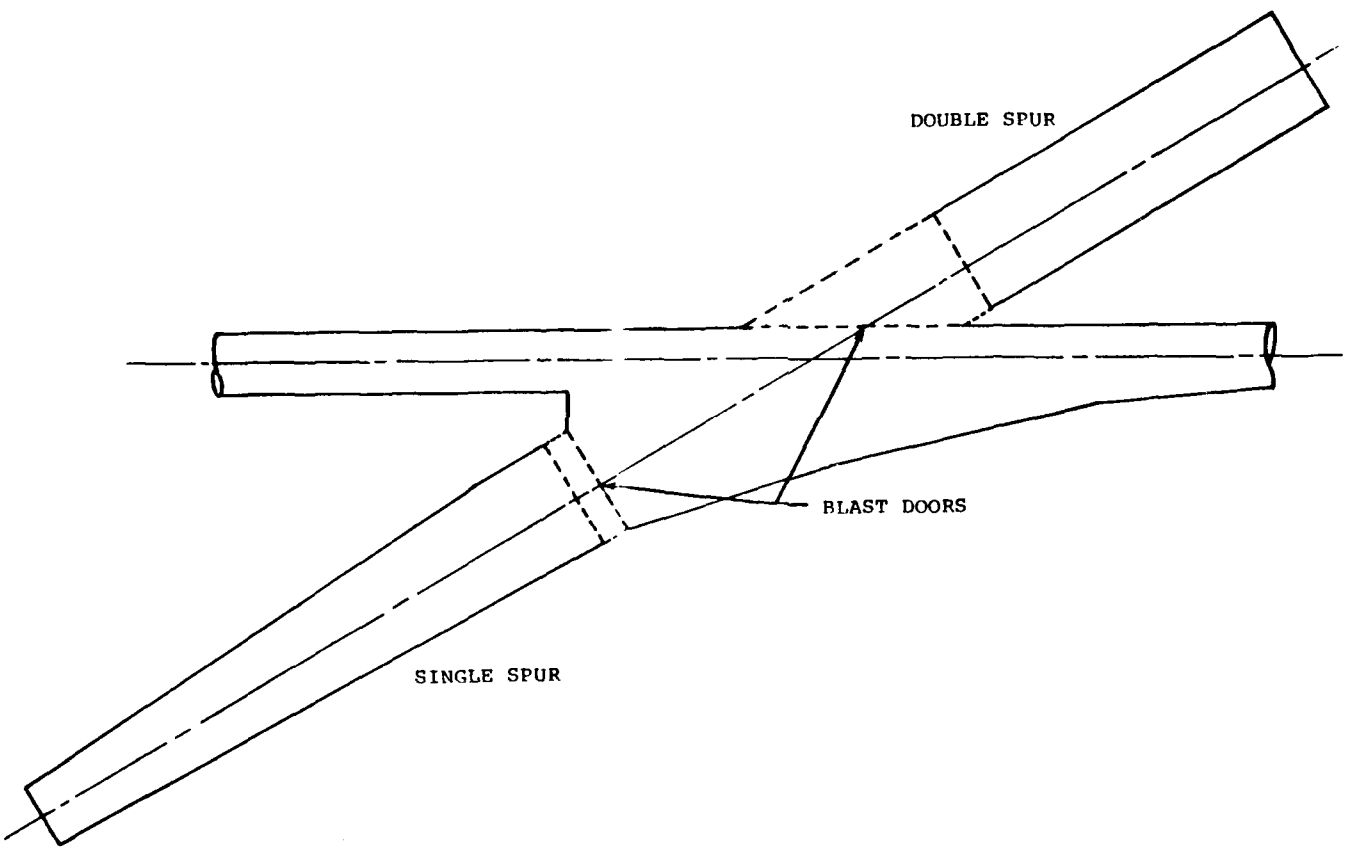

FIGURE 1. M-X TRENCH OFF-LINE BASING CONCEPTS

2.0 SHOCK TUBE TEST PROGRAM

A series of shock tube experiments were conducted at NASA Ames Research Center Electric Arc Shock Tube (EAST) to aid in the understanding of airblast propagation in the M-X spur. The facility was selected because of its ability to produce strong, repeatable shock waves at ambient or near ambient initial pressures.

The M-X spur test section was attached to the EAST facility and tested at an initial shock strength of P_{21} = 40 after facility calibration tests. Pressure measurements were obtained on the blast door and at other selected points in the model.

2.1 Model and Instrumentation

The M-X spur test section is a 1:33 geometrically scaled model. A clam shell design was used to obtain the internal rectangular geometry which was cut from the three inch thick aluminum ingots used for the top and bottom halves of the test section. The clam shell test section was clamped with nineteen 2 1/8" diameter bolts (Figure 2) so that the internal pressure (1000 psi) could be contained. Four tirods were used for strength along both the shock tube and spur turnout axes (Figure 3).

Tangent type circular to square junctions were used at each end of the test section. Throughout the test section the top and bottom walls form parallel planes with a spacing (10 cm) equivalent to the shock tube diameter. All of the sidewalls between the circular to square junctions and those in the spur turnout were planar. The coordinates of the inside walls are defined with respect to an origin located at the intersection of the shock tube and spur turnout axes (Figure 4).

Pressure measurements were made at 16 stations located on the blast plug wall, the roof, the adjacent wall, and in the turnout (Figure 5). The station coordinates are listed in Table

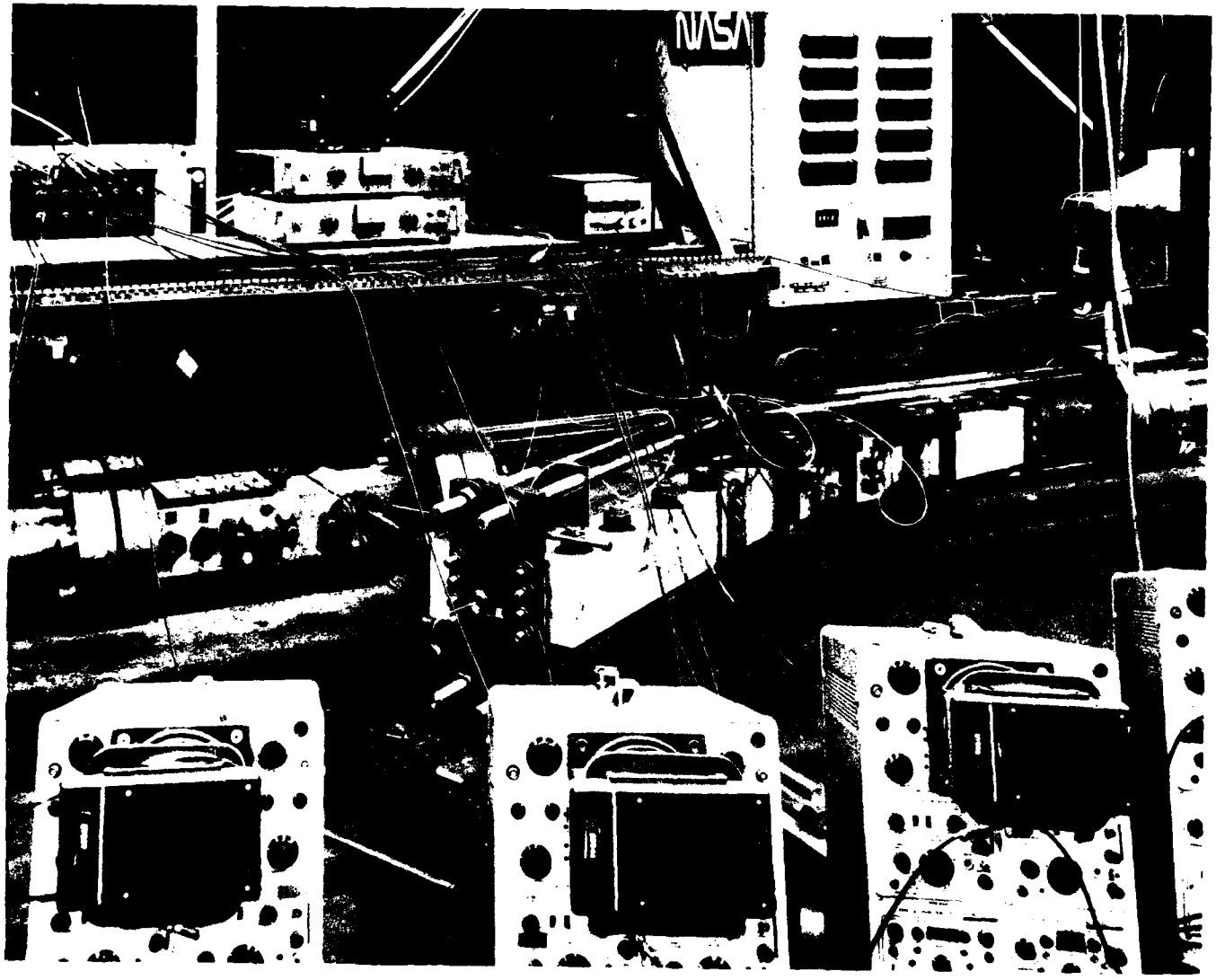

FIGURE 2. CLAM-SHELL TEST SECTION INSTALLATION IN EAST FACILITY (NASA/AMES RESEARCH CENTER)

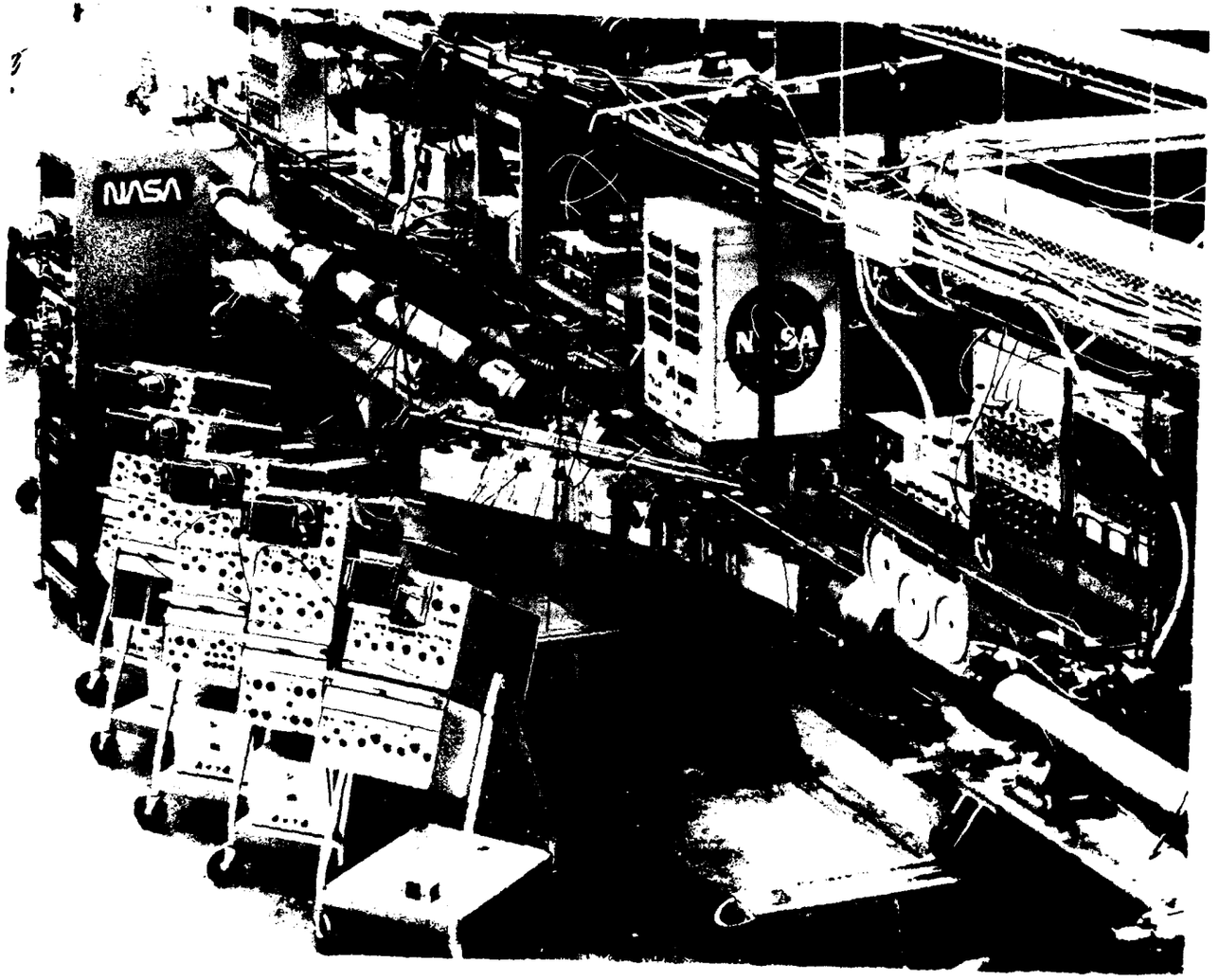

FIGURE 3. M-X DOUBLE SPUR MODEL TEST ASSEMBLY

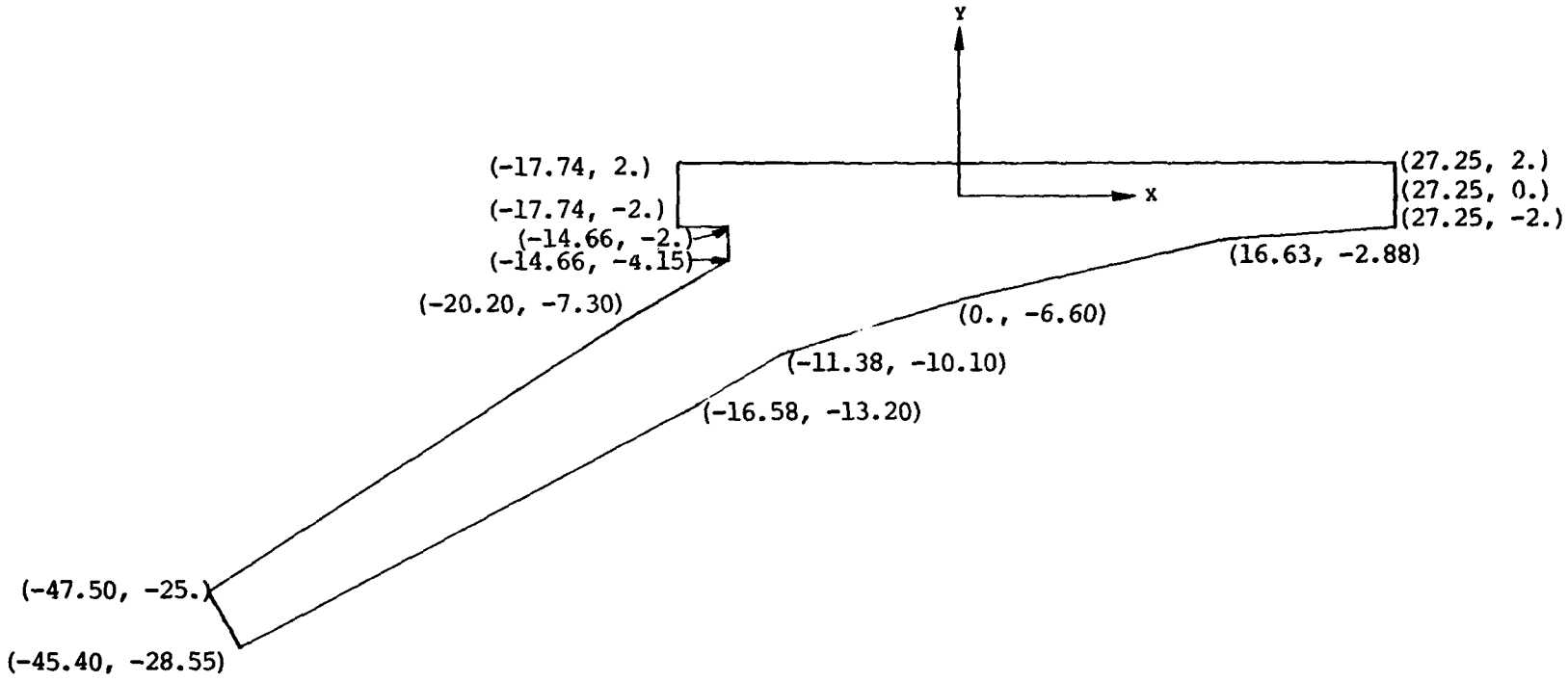

FIGURE 4. M-X SPUR DIMENSIONS (COORDINATES IN INCHES)

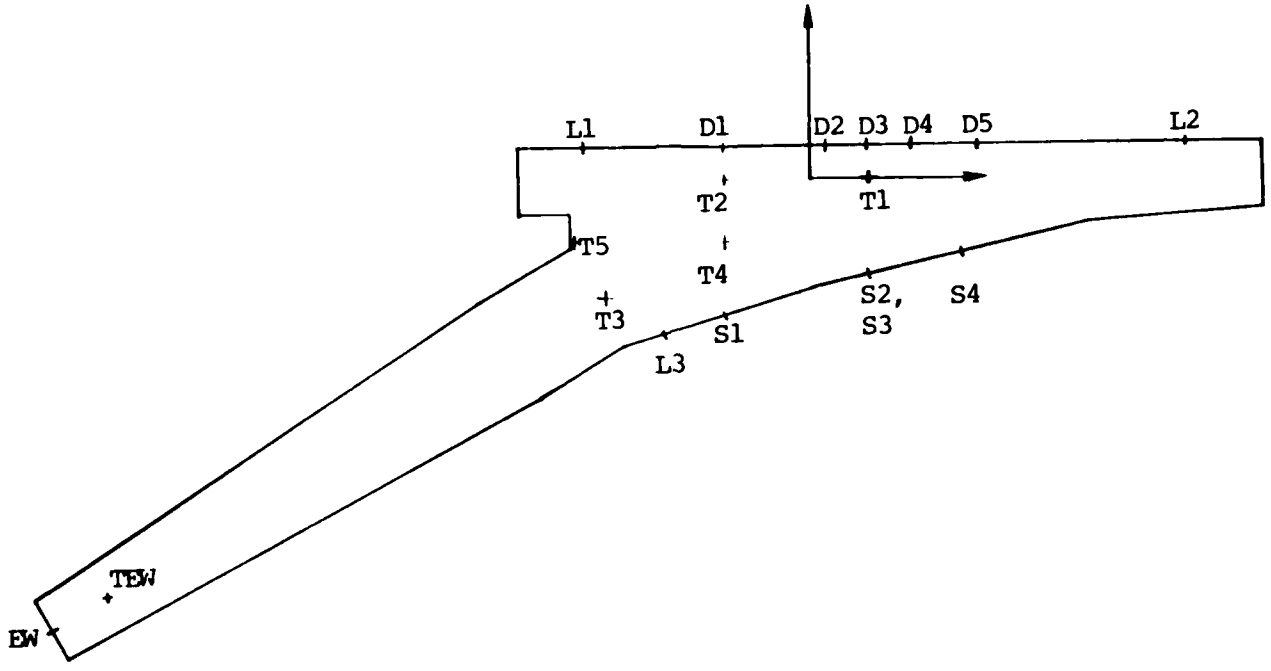

FIGURE 5. PRESSURE MEASUREMENT STATIONS

TABLE 1. INSTRUMENTATION STATION COORDINATES

Station	Coordinates (X,Y)
L2	(22.80, 2.00)
D5	(10.20, 2.00)
D4	(6.05, 2.00)
D3	(3.55, 2.00)
D2	(0.93, 2.00)
D1	(-5.25, 2.00)
L1	(-13.70, 2.00)
T1	(3.55, 0.00)
T2	(-5.25, 0.00)
T3	(-12.40, -7.19)
T4	(-5.25, -3.75)
T5	(-14.52, -3.75)
EW	(-46.40, -26.80)
TEW	(-43.00, -24.80)
L3	(-8.90, -9.30)
S1	(-5.25, -8.20)
S2,S3	(3.55, -5.76)
S4	(9.18, -4.40)

1. Stations D2, D3, and D4 are located on the blast plug whereas stations D1 and D5 are located on each side of the blast plug. Pcb Piezotronics pressure transducers models 113A22 and 113A24 were flush mounted in steel inserts in the side wall. The transducers were protected from the thermal environment by covering the transducer face with a thin layer of commercial RTV.

2.2 Facility Description

The NASA Ames Research EAST facility (Figure 6) is an electric arc shock tube used for high energy shock physics experiments. EAST consists of a 1.2 MJ capacitor bank, an 0.1 meter I.D. shock tube and a dump tank (Figure 7). For the present tests a 1.36 meter long cylindrical driver was employed.

Strong shocks are created by discharging energies approaching 1 MJ into a driver section through an exploding wire technique. Joule heating of the driver gas takes place when an arc is struck along the wire path betweeen the ground electrode at the diaphragm station and the high voltage electrode at the base of the driver (Figure 8). Alternate gases such as helium are used in the driver section to create stronger shocks than would occur with air in the driver. Details of the driver operation can be found in References 1 and 2.

Operation of the shock tube is easily illustrated by considering a constant diameter tube divided into two regions: a high pressure driver section and a lower pressure driven section separated by a diaphragm (Figure 9a). When the diaphragm is burst, a shock wave propagates down the driven section, and an expansion fan propagates back into the driver section (Figure 9b). The expansion fan converts the stagnation energy of the driver gas into flow energy (of the expanded driven gas) and compressive work (which accelerates the driver gas). Expansion waves travel at the speed of sound relative to the local driver gas conditions; thus the driver gas sound speed is an important

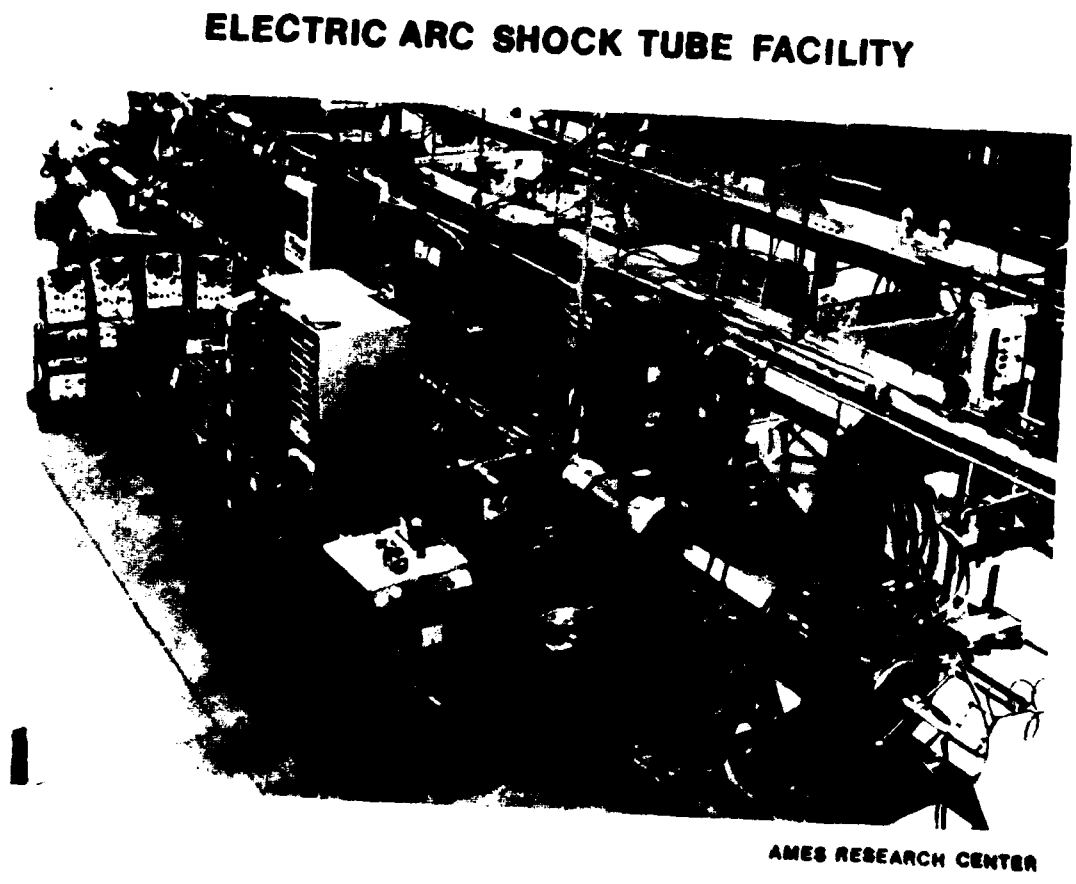

FIGURE 6. EAST FACILITY.

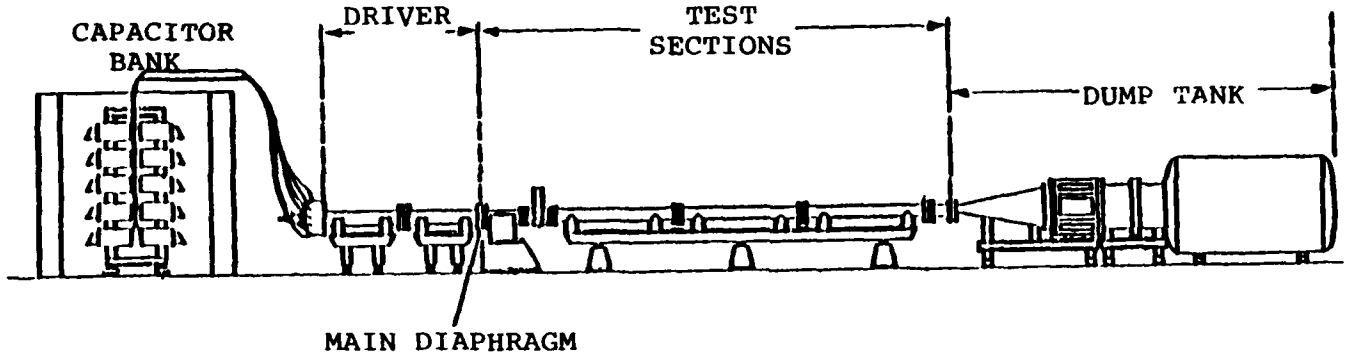

FIGURE 7. NASA AMES ELECTRIC ARC SHOCK TUBE SCHEMATIC.

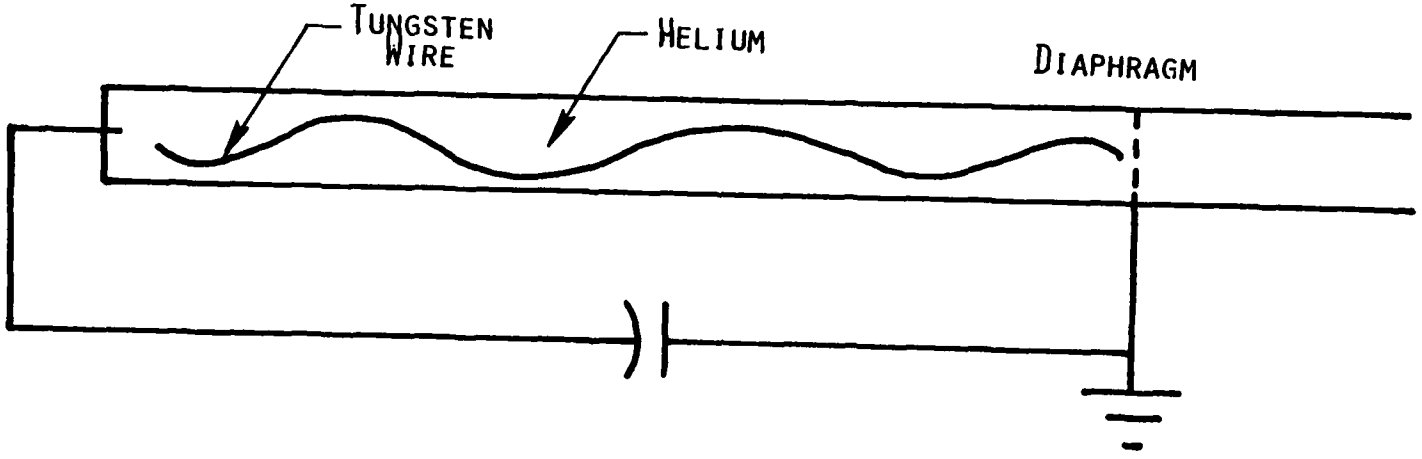

CAPACITOR BANK

C = 1520 μFARADS
VOLTAGE = 0 - 40. K VOLT
ENERGY = 0 - 1.2 M JOULE

FIGURE 8. ARC HEATED DRIVER.

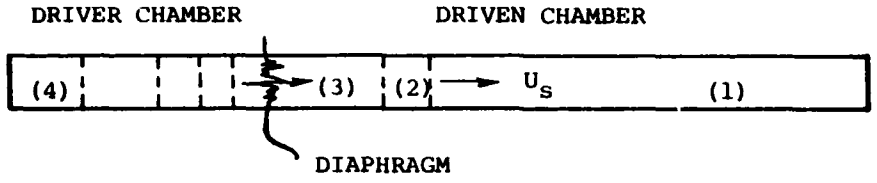

FIGURE 9A. SHOCK TUBE SCHEMATIC.

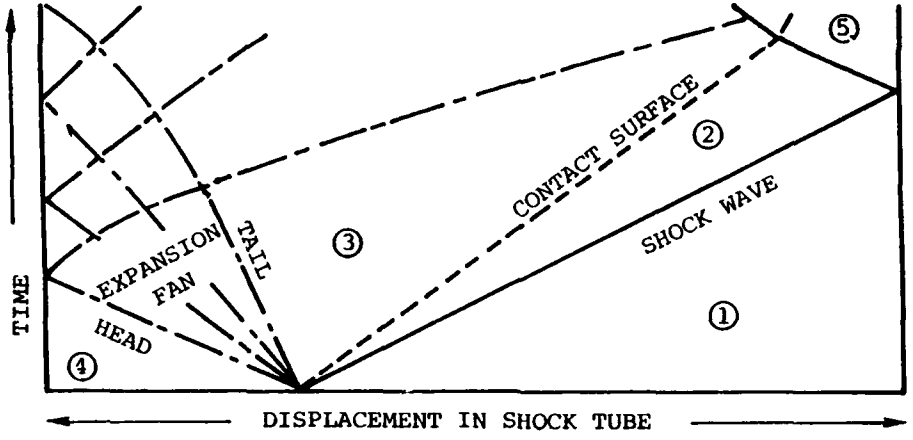

FIGURE 9B. SHOCK TUBE X-T DIAGRAM.

parameter in creating strong shocks. References 3 and 4 present the details of shock tube performance.

Using the notation of Figure 9, the ideal shock Mach number is determined from

$$P_{41} = \frac{1 + \frac{2\gamma_1}{\gamma_1 + 1}\left(M_s^2 - 1\right)}{\left(1 - \frac{\left(\gamma_4 - 1\right)\left(M_s^2 - 1\right)}{\left(\gamma_1 + 1\right)A_{41}M_s}\right)^{\frac{2\gamma_4}{\gamma_4 - 1}}} \tag{1}$$

where A is sound speed and the double subscript implies a ratio. The shock pressure ratio or strength is

$$P_{21} = \frac{2\gamma_1}{\gamma_1 + 1}\left(M_s^2 - 1\right) + 1 \tag{2}$$

Driver gas (Region 4) state after arc discharge is estimated from the constant volume heating law of thermodynamics for ideal gases

$$P_{41} = T_{41} = 1 + \left(\gamma_4 - 1\right)\left(\frac{E}{VP_{4i}}\right) \tag{3}$$

$$A_{41} = \left(\frac{\gamma_{41}}{m_{41}} T_{41}\right)^{\frac{1}{2}} \tag{4}$$

where m is the molecular weight. Equations 1 through 4 were used to estimate the shock tube performance. Final test conditions were selected from one-dimensional finite difference calculations (SAI's RIST Code, Reference 5) and verified in calibration runs.

3.0 EXPERIMENT RESULTS

Ten runs were made in the NASA EAST facility to investigate the propagation of strong shocks (P_{21} - 40) in a model of the M-X Double Spur. Calibration runs established the shock wave characteristics in the existing smooth wall NASA shock tube and determined the arc driver performance. The SPUR model was then installed such that the blast door was centered about the 52 diameter station. Since the M-X DOUBLE SPUR is asymmetric, the model was tested in both orientations first in the FLOW-PAST-SPUR and then in the FLOW-INTO-SPUR configuration. Pressure histories were measured at various points in the Spur model. Specific locations were selected either because they represent a point of vulnerability, for example the blast door, or because the wave propagation about the point was helpful to interpret the data.

3.1 Calibration of Shock Tube

Shock wave characteristics in the smooth walled NASA shock tube were selected from finite differnce calculations to satisfy several constraints:

a) obtain a pressure history at the test section which displays a 1 msec constant pressure duration so that incident pressure decay would not cloud data interpretation,

b) match acoustic impedance across contact surface to avoid reflected shock interactions with an impedance mismatch,

c) and for structural integrety limit the maximum internal pressure to 1000 psi; thereby restricting the initial test section pressure to ½ atmosphere.

The 1.37 meter driver section was filled with Nitrogen at P_{4i} = 18 atm while the test section contained air at P_1 = 0.5 atm. Both sections were at room temperature (T = 300^{0}K). After the arc discharge, the theoretical driver conditions were P_4 = 378 atm

and T_4 = 6300°K assuming an ideal gas equation of state and that the arc discharge transfered 100% of the stored electrical energy to the driver gas which should produce a shock Mach number of 6.8 (P_{21} = 53) as is shown in Figure 10. The actual shock tube performance is expected to be lower because the energy transfer efficiency is nominally 70% and because real gas effects cause an additional limit on the temperature rise.

To calibrate the shock tube the pressure histories were recorded at stations 20, 40, and 52. The desired shock strength of P_{21} = 40 was observed at station 52 (Figure 10) and a nominal decay of 5% was observed between stations 40 and 52. The pressure histories displayed a constant pressure duration which exceeded the desired duration of 1 msec. The duration of the shocked gas is much shorter; infact at station 40 the test time was 100 μsec (Figure 11) which would indicate that for this shock speed C_S = 2.0 km/sec the contact surface was located about 20 cm behind the shock. Since the contact surface would enter the Spur model during the initial portion of the test it was crucial to have matched acoustic impedance to avoid reflected wave refractions at the interface. The calibrated shock tube performance satisfied all constraints required for the Spur tests and was used for the tests with the model in place.

3.2 Measurements in the Spur Model

With the calibration runs complete the test section was installed in the EAST facility. For both FLOW-PAST-SPUR and FLOW-INTO-SPUR configurations the blast door was centered about the 52 diameter station where the shock strength at the equivalent point in the smooth tube was P_{21} = 40. Pressure histories were measured on the blast door, the adjacent wall, the roof, and the turnout, and the exact measurement stations are identified in Figure 5 and located in Table 1.

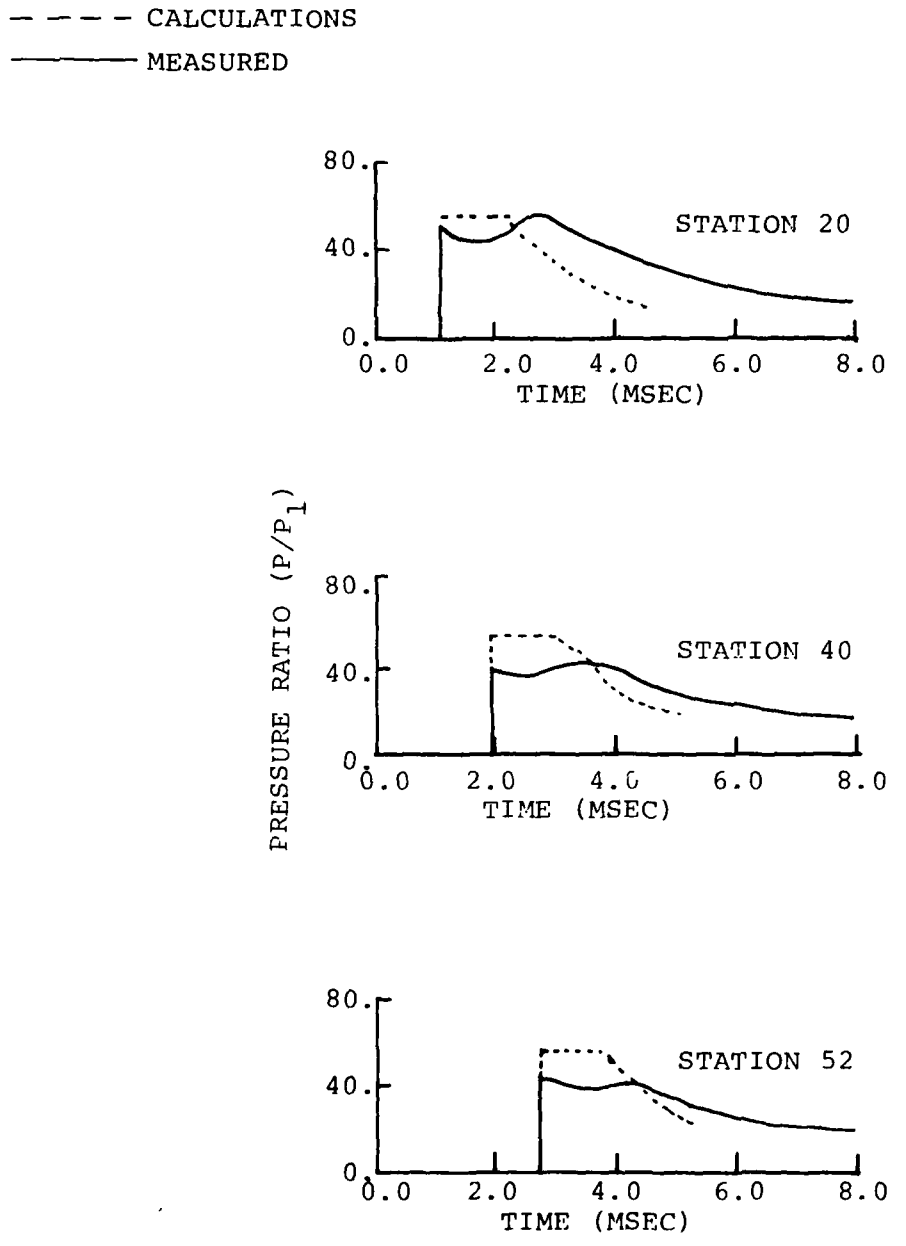

FIGURE 10. SELECTION OF TEST CONDITIONS - PRETEST CALCULATIONS AND CALIBRATION RUN MEASUREMENTS.

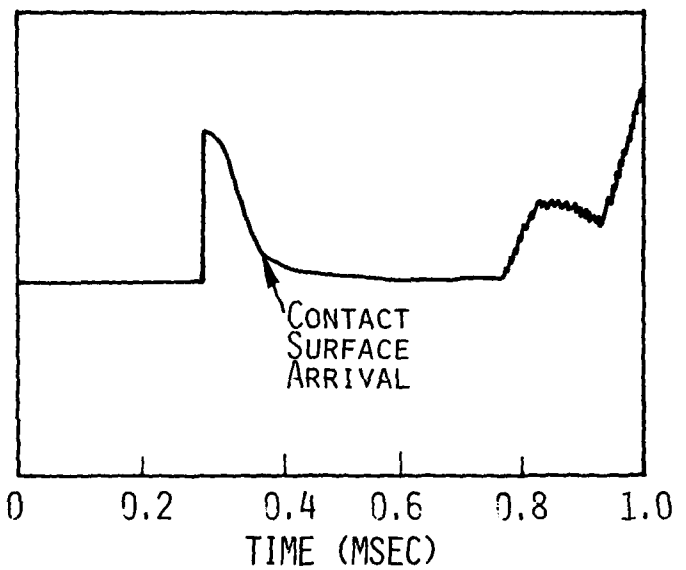

FIGURE 11. SHOCKED GAS TEST TIME IN AIR AT THE 40 DIAMETER STATION (P_1 = 0.5 ATM, M_s = 6.0)

3.2.1 Flow Past Spur

Pressure histories along the blast door wall (Figure 12) display the arrival of the incident shock and the wave reflected off the adjacent wall. The reflected wave arrived 4.0 msec after the incident shock at station D1. At stations D2 through D5 the reflected wave arrival varies from 0.5 msec to 0.1 msec, respectively, after the incident shock. The initial shock strength decreases as it passes across the blast plug because the wave reflected off the converging adjacent wall has not passed back across to the blast plug. However when the reflected wave does reach the blast plug, the convergence causes its strength to increase in the downstream direction (Figure 13).

Pressure histories along the adjacent wall exhibit a rapid pressure decay behind the shock (Figure 14). The duration of the peak varies from 100 μsec at station S1 to 50 μsec at Station S4. The pressure histories at later times exhibit gradual changes. At Station S1 the pressure is constant, and at Station S4 a slow compression is observed to peak at 1.5 msec after shock wave arrival.

The initial shock pressure ratio on the wall across to the blast plug (Figure 15) is considerably higher than the pressure ratio at other points in the Spur because of its inclination to the tube axis (Figure 4). Interestingly, the maximum pressure occurs directly across from the blast plug.

Pressure histories on the Spur roof (Figure 16) show that the decaying initial shock is followed by the reflected wave off the wall across from the blast plug. At stations T1 and T2, the reflected wave arrives 300 μsec after the initial shock and is observed to be followed by its reflection off the blast plug.

The initial shock pressure ratio on the Spur roof follows the decay observed along the blast plug wall until the shock

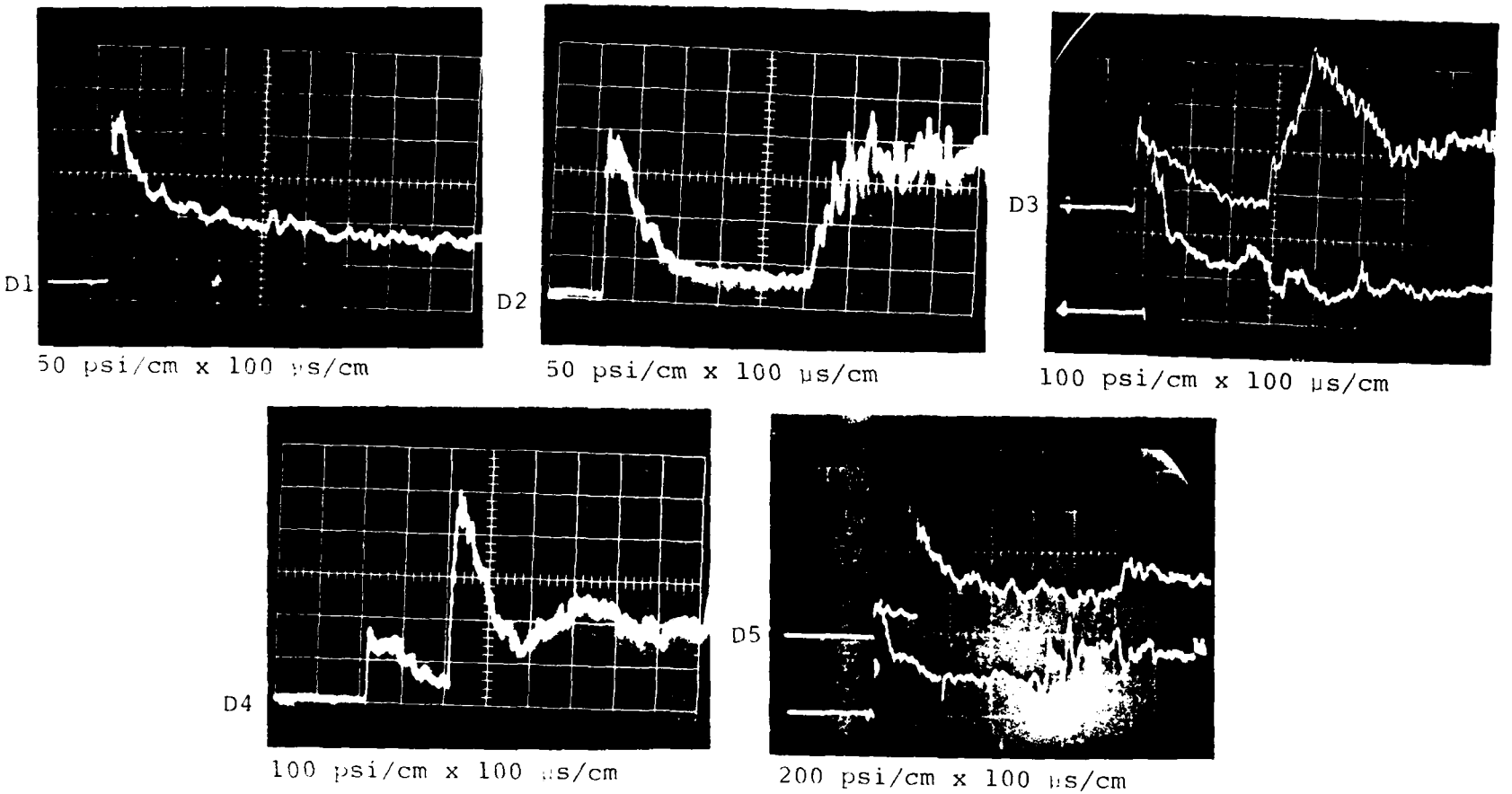

FIGURE 12. FLOW-PAST-SPUR PRESSURE HISTORIES ON THE BLAST DOOR (STATIONS D1 THROUGH D5)

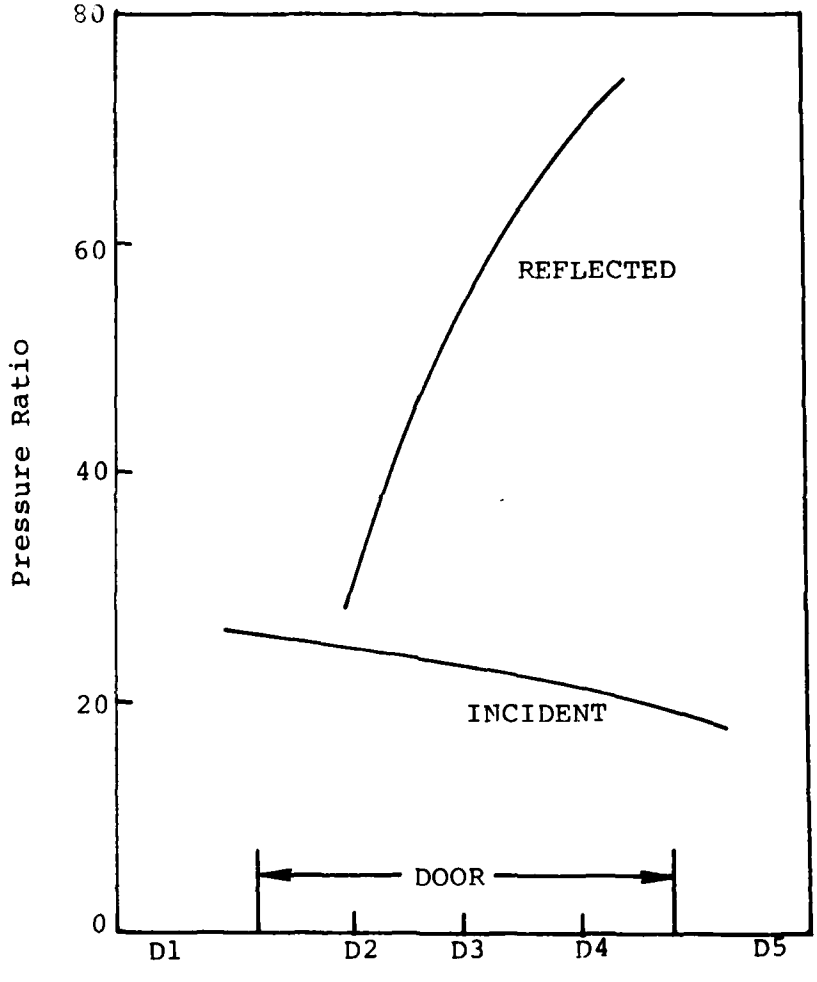

FIGURE 13. FLOW-PAST-SPUR SHOCK PRESSURES ON THE BLAST DOOR

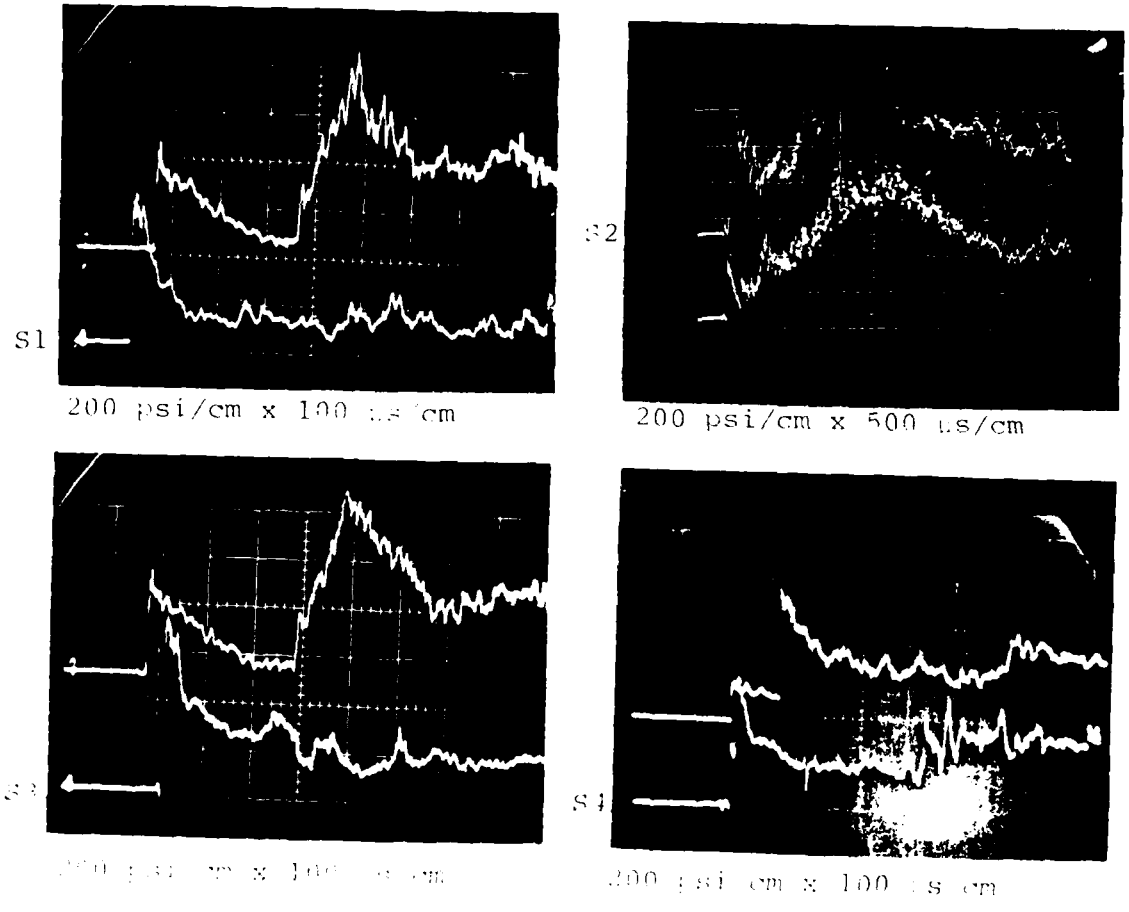

FIGURE 14. FLOW-PAST-SPUR PRESSURE HISTORIES ON CONVERGENT WALL (STATIONS 51 THROUGH 54)

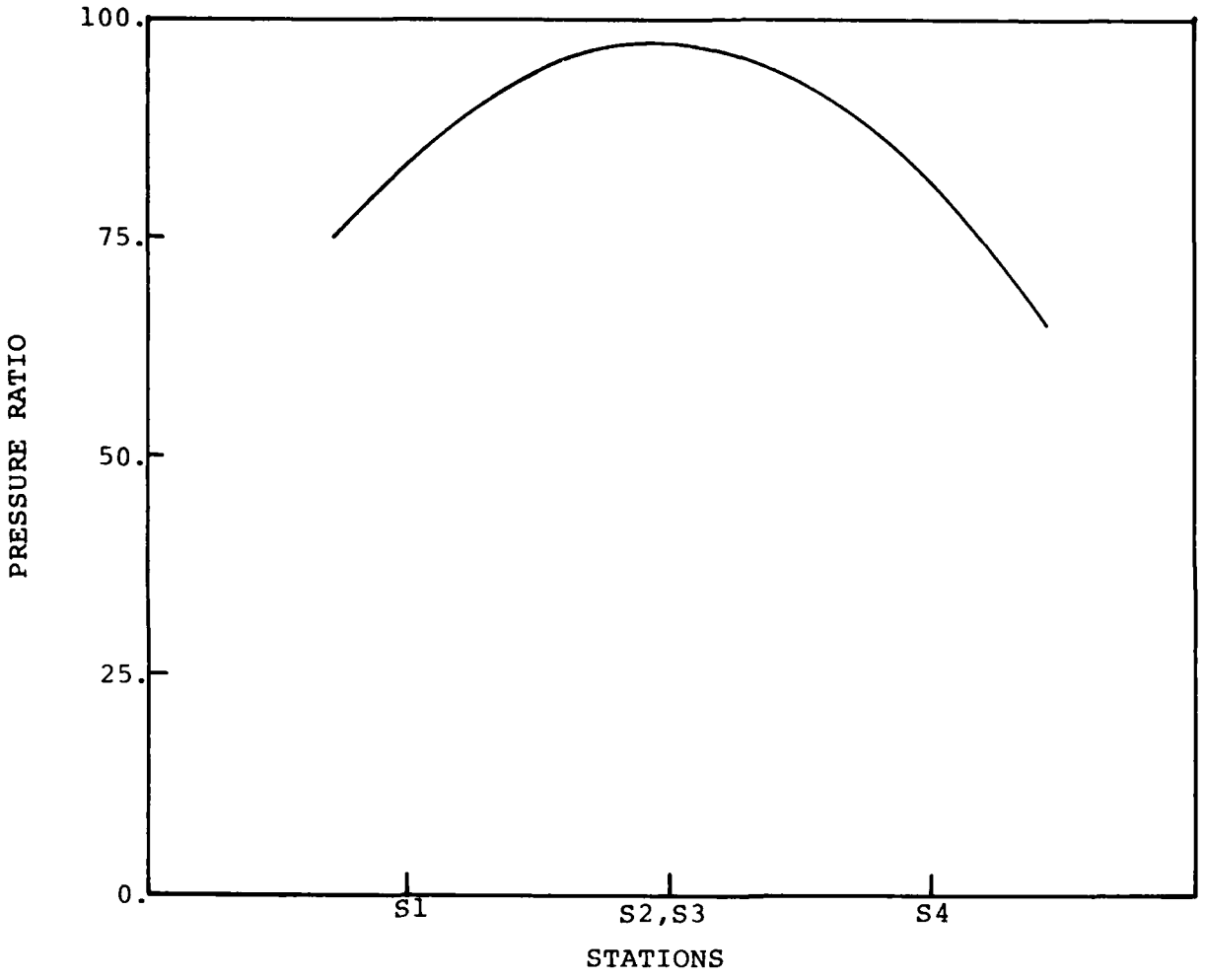

FIGURE 15. FLOW-PAST-SPUR SHOCK PRESSURES ON CONVERGENT WALL.

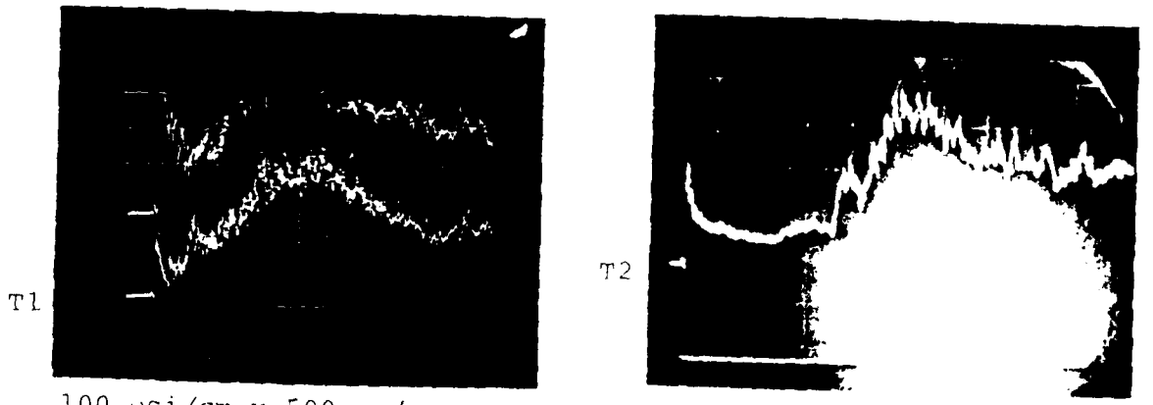

FIGURE 16. FLOW-PAST-SPUR PRESSURE HISTORIES ON SPUR ROOF (STATIONS T1 AND T2)

reaches the center of the blast plug. At Station T1 the pressure ratio is about 80 percent of the initial shock pressure on the center of the blast plug (D3).

Pressure histories in the Spur turnout (Figure 17) show two rather weak shocks reach the end wall (Station EW) with a spacing of 1.5 msec. The end wall reflected pressure ratio for the incident shock is P_{21} = 28. The following shock whose origin must be associated with the convergence in the downstream portion of the Spur almost doubles the pressure on the endwall (P/P_1 = 50).

3.2.2 Flow into Spur

Four runs were performed with the test section installed in the FLOW INTO SPUR configuration. In this orientation the tube crossectional area transitions smoothly from the shock tube to the gradually increasing area of the channel along the blast plug (Figure 4). As the incident shock passes along the blast plug a peaked waveform is observed (Figure 18). The decay to half maximum is about 200 μsec.

A portion of the incident shock passes into the turnout, and after reflecting off the end of the turnout returns toward the blast plug. The series of reflected waves begin arriving at station D1 at 2.2 msec and at Station D5 at 3.0 msec after the incident shock. The incident shock strength decays as it crosses the blast plug (Figure 19) and is observed to be P_{21} = 30 on the center of the blast plug. The reflected waves strengthen as they pass upstream; in fact at Station D3 the pressure peaks are observed to be P/P_1 = 70.

The pressure waveforms on the wall adjacent to the blast plug also exhibit a preaked initial wave followed by a series of waves reflected out of the turnout (Figure 20). At Station S3 the reflected waves begin arriving about 2.5 msec after the initial shock. The initial shock strength at Station S3 is P_{21} = 30 as is the reflected shock strength.

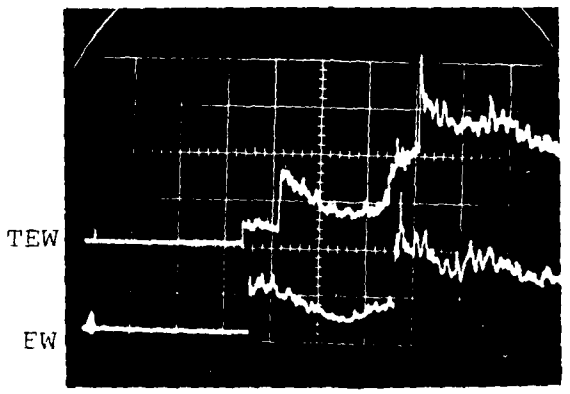

FIGURE 17. FLOW-PAST-SPUR PRESSURE HISTORIES IN TURNOUT (STATIONS TEW AND EW)

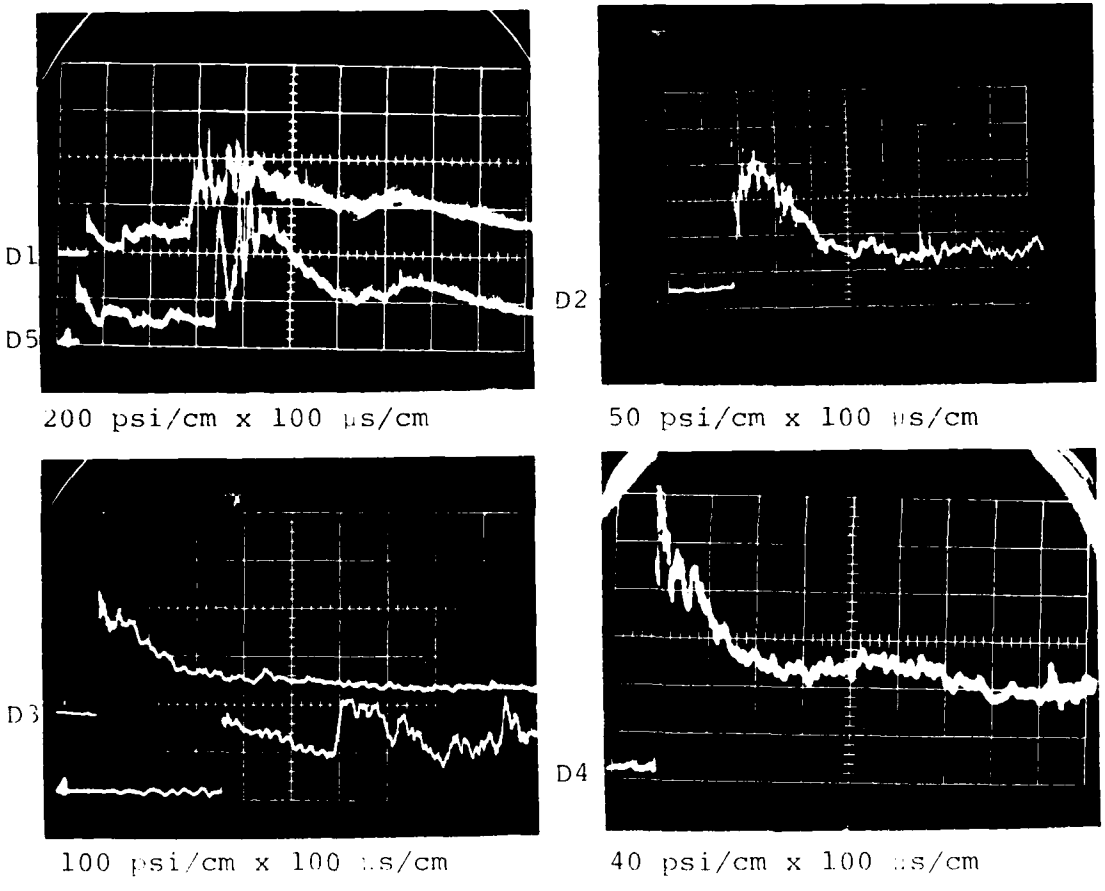

FIGURE 18. FLOW-INTO-SPUR PRESSURE HISTORIES ON BLAST DOOR (STATIONS D1 THROUGH D5)

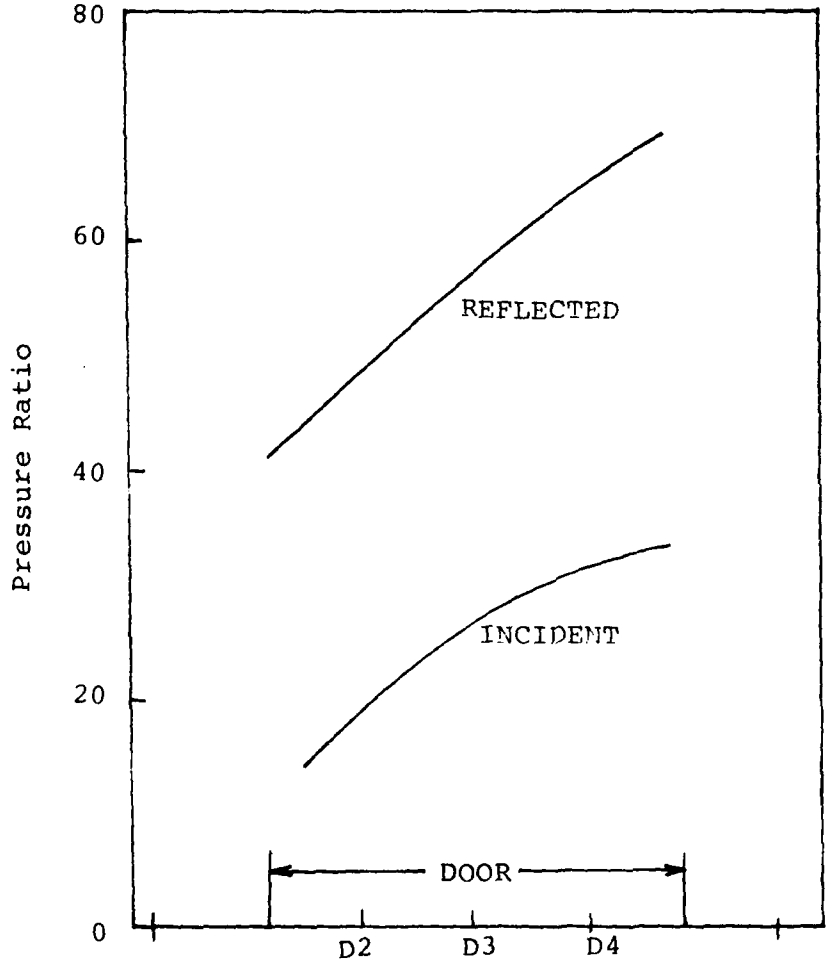

FIGURE 19. FLOW-INTO-SPUR SHOCK PRESSURES ON BLAST DOOR

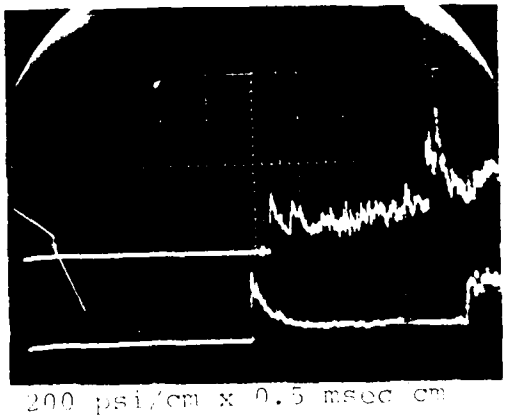

FIGURE 20. FLOW-INTO-SPUR PRESSURE HISTORIES ON CONVERGENT WALL (STATION 53)

The pressure waveforms on the roof (Stations T2 and T3) exhibit a peaked initial wave followed by a series of waves reflected out of the turnout (Figure 21). The pressure waveform at Station T5 exhibits the reflection of the initial wave off the wall between the tunnel and the turnout (Figure 5). Again a rather strong reflected wave with considerable duration is observed to arrive about 2.5 ms after the initial shock.

The initial shock strength at Station T2 is $P_{21} = 25.8$ and decays to $P_{21} = 19.0$ at Station T3. Normal reflection at Station T5 creats a shock strength of $P/P_1 = 129$.

Pressure waveforms were recorded at Stations TEW and EW in the turnout. The initial shock observed at Station TEW is followed closely by two rather weak shocks (Figure 22), and the reflected shock returns at 220 μsec. The pressure signal from Station EW displayed some spurious noise for about one millisecond after shock wave arrival which may have been caused by vibration in the end wall. Although the signal was noisy it could be interpreted at late times and in fact the reflected pressure appeared to agree with the later time measurement at Station TEW.

The initial shock strength was observed to be $P_{21} = 20$ at Station TEW, and at both Stations TEW and EW the reflected pressure ratio was observed to be $P/P_1 = 160$.

3.3 Comparison with Calculations

Two calculations of airblast propagation into the M-X Spur were compared to the measured data obtained in the NASA/SAI test series. The calculations were performed by TRW (Reference 6) and Systems Science and Software (Reference 7) and both used incident shock strengths of 40. However the flow behind the incident shock was not equivalent to that obtained in the EAST facility. The TRW calculations were of a 1 megaton surface burst at an 1800

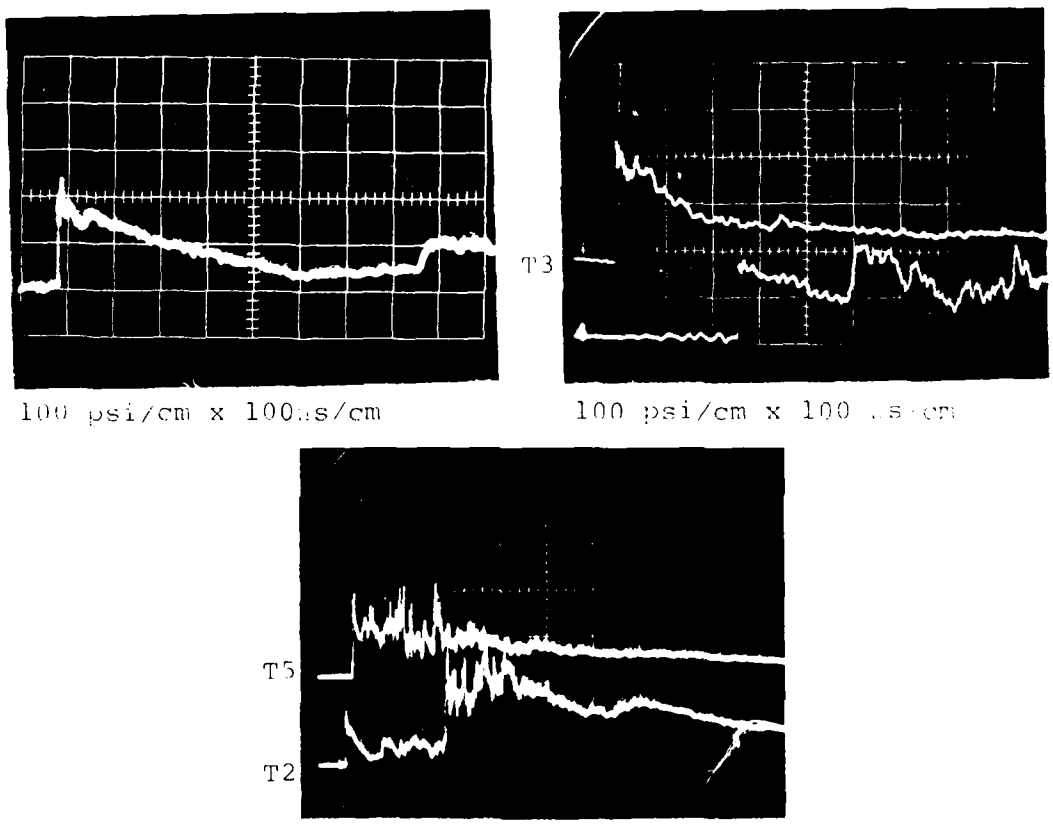

FIGURE 21. FLOW-INTO-SPUR PRESSURE HISTORIES ON ROOF (STATIONS T2, T3, AND T5)

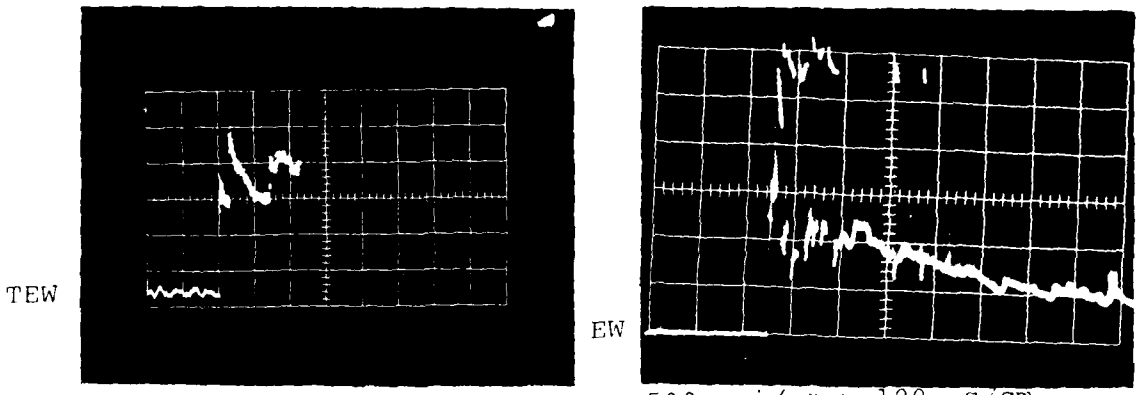

FIGURE 22 FLOW-INTO-SPUR PRESSURE HISTORIES IN TURNOUT
(STATIONS EW AND TEW)

foot range which produced a 40 bar peaked wave at the Spur. The TRW calculations were performed only for the FLOW-PAST-SPUR configurations. Systems, Science and Software calculations were of the explosive driver tests performed at Stanford Research Institute (Reference 8) and considered airblast loading from both directions.

For the FLOW-PAST-SPUR configuration most of the important wave propagation occurs near the initial shock and is therfore less dependent on the late time flow. The excellent agreement shown in the limited comparison of Figure 23A indicates that despite late time differences the flow near the initial shock is equivalent. The calculated reflected wave pressures on the blast door varied in the same manner as the measured values.

For the FLOW-INTO-SPUR configuration the important wave propagation endures for a much longer time and consequently the effects of the late time flows are more important. The disagreement shown in Figure 23B could be expected and indicates that the calculated reflected shock pressures were almost a factor of two below measured values. The significance of the late time flow can only be quantitatively discussed with a proper set of calculations.

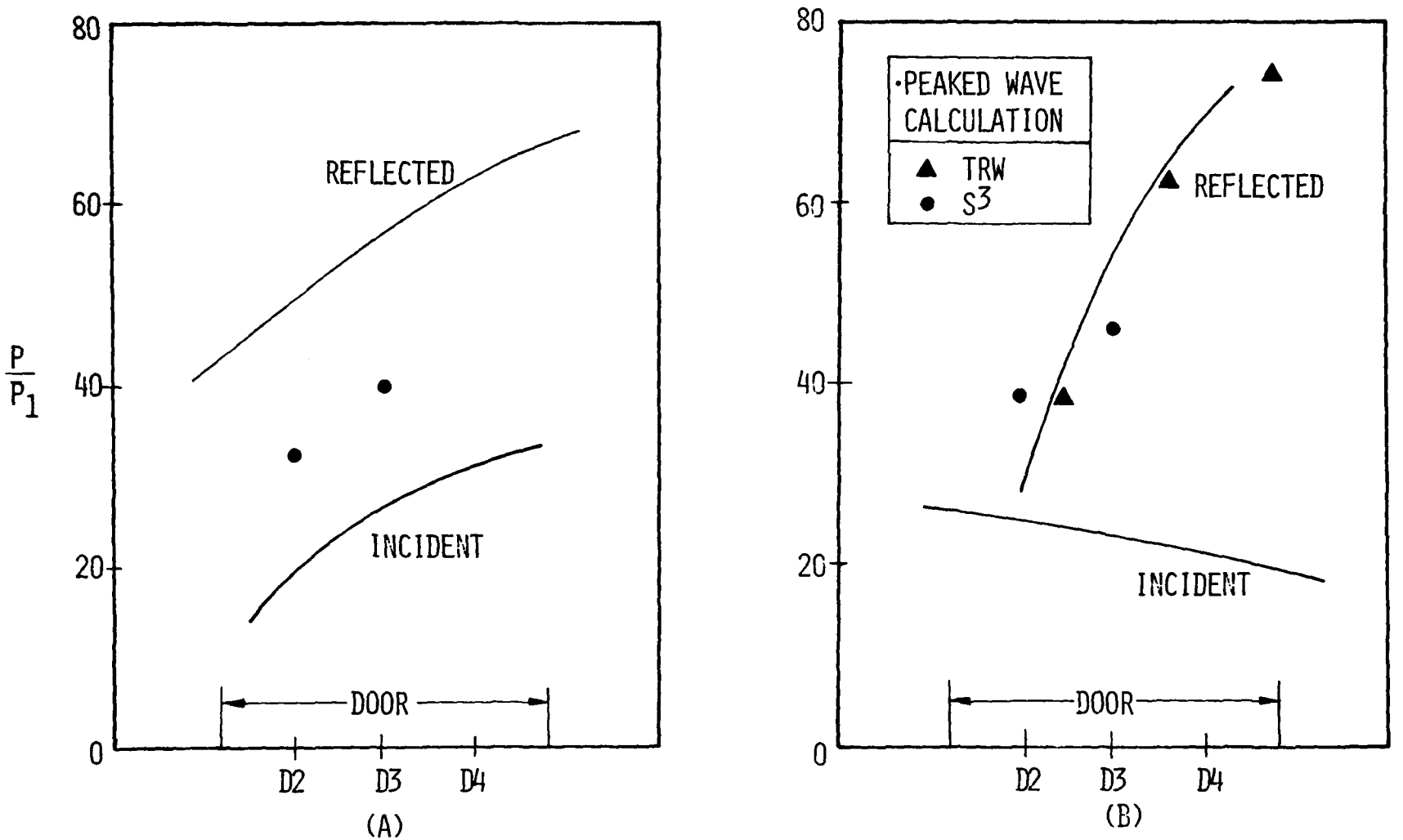

FIGURE 23. COMPARISON OF MEASURED AND PREDICTED SHOCK PRESSURES ON THE BLAST DOOR FOR FLOW-INTO-SPUR (A) AND FLOW-PAST-SPUR (B) LOADING CONDITIONS

4.0 SUMMARY

The M-X double spur model was tested in both orientations with a square incident shock. Pressure histories were measured at various points in the model.

The major observations for the FLOW-PAST-SPUR tests are:

- the initial shock strength on the blast door $P_{21} \sim 25.$ is slightly lower than the strength of the incident test shock in the shock tube.
- the reflection of the initial shock along the convergent wall creates a reflected wave which impinges upon the blast door. This impinging shock produces the highest loads on the blast door ($P_{57} = 60$).
- the shock strength of the wave in the turnout is quite weak ($P_{21} \sim 10.$).

The major observations for the FLOW-INTO-SPUR tests are:

- the initial shock strength on the blast door $P_{21} \sim 30$ is slightly lower than the strength of the incident test shock in the shock tube.
- a portion of the initial shock passes into the turnout and at the end reflects up to a high pressure $P/P_1 \sim 130$.
- the reflected wave returns through the turnout and impinges on the blast door producing a pressure of $P/P_1 \sim 60$.

Comparison of measured results with calculations revealed that:

- for the FLOW-PAST-SPUR tests, calculated initial and reflected shock pressures are in good agreement with measurements.
- for the FLOW-INTO-SPUR tests, measured reflected shock pressures are higher than calculated values; however calculations were not performed specifically for the NASA test conditions.

To interpret the differences in the late time flow it is recommended that the disparity in the incident waveform be eliminated by performing calculations of the NASA test conditions.

REFERENCES

1. "Arc Driver Operation for Either Efficient Energy Transfer or High-Current Generation," R. E. Dannenberg and A. F. Silva, *AIAA Journal*, Vol. 10, No. 12, December 1972, pp. 1563-1564.

2. "Development of Dynamic Discharge Arc Driver with Computer Aided Circuit Simulation," R. E. Dannenberg and P. I. Slapnicar, *AIAA Journal*, Vol. 14, No. 9, September 1976 pp. 1183-1188.

3. "Handbook of Supersonic Aerodynamics, Section 18, Shock Tubes," I. I. Glass and J. G. Hall, NAVORD Report 1488 (Vol. 6), December 1959.

4. "Principles and Applications of Shock Tubes and Shock Tunnels," NASA TM-X-69941, October 1963.

5. "RIST Code Operation," R. Issa, SAI IOC LAC-780-077, October 1972.

6. Personal communication with T. Mazzola at TRW, March 1978

7. Personal communication with Dr. Kedar D. Pyatt, Jr., Systems, Science and Software, May 1978.

8. Personal communication with Dr. Jim Colton, Stanford Research Institute, May 1978.

DISTRIBUTION LIST

DEPARTMENT OF DEFENSE

Assistant to the Secretary of Defense
Atomic Energy
ATTN: Executive Assistant

Defense Advanced Rsch. Proj. Agency
ATTN: TIO

Defense Intelligence Agency
ATTN: RDS-3A

Defense Nuclear Agency
ATTN: SPSS, G. Ullrich
ATTN: SPSS, E. Sevin
ATTN: DDST
3 cy ATTN: SPSS, J. Galloway
4 cy ATTN: TITL

Defense Technical Information Center
12 cy ATTN: DD

Field Command
Defense Nuclear Agency
ATTN: FCPR
ATTN: FCTMD

Field Command
Defense Nuclear Agency
Livermore Division
ATTN: FCPRL

Joint Strat. Tgt. Planning Staff
ATTN: NRI-STINFOR Library
ATTN: XPFS

Undersecretary of Def. for Rsch. & Engrg.
ATTN: Strategic & Space Systems (OS)

DEPARTMENT OF THE ARMY

BMD Advanced Technology Center
Department of the Army
ATTN: ATC-T

Chief of Engineers
Department of the Army
ATTN: DAEN-ASI-L
ATTN: DAEN-MPE-T, D. Reynolds
ATTN: DAEN-RDL
ATTN: DAEN-RDM

Harry Diamond Laboratories
Department of the Army
ATTN: DELHD-I-TL
ATTN: DELHD-N-P

U.S. Army Ballistic Research Labs.
ATTN: DRDAR-TSB-S
ATTN: DRDAR-BLE, J. Keefer

U.S. Army Cold Region Res. Engr. Lab.
ATTN: Library

DEPARTMENT OF THE ARMY (Continued)

U.S. Army Construction Engrg. Res. Lab.
ATTN: Library

U.S. Army Engineer Center
ATTN: Technical Library

U.S. Army Engr. Waterways Exper. Station
ATTN: Library
ATTN: WESSA, W. Flathau
ATTN: WESSD, G. Jackson

U.S. Army Material & Mechanics Rsch. Ctr.
ATTN: Technical Library

U.S. Army Materiel Dev. & Readiness Cmd.
ATTN: DRXAM-TL

U.S. Army Nuclear & Chemical Agency
ATTN: Library

DEPARTMENT OF THE NAVY

Naval Construction Battalion Center
ATTN: Code L08A
ATTN: Code L51, J. Crawford
ATTN: Code L53, J. Forrest

Naval Facilities Engineering Command
ATTN: Code 09M22C

Naval Postgraduate School
ATTN: G. Lindsay
ATTN: Code 0142

Naval Research Laboratory
ATTN: Code 2627

Naval Surface Weapons Center
ATTN: Code X211
ATTN: Code F31

Naval Surface Weapons Center
ATTN: Tech. Library & Info. Services Branch

Office of Naval Research
ATTN: Code 715

DEPARTMENT OF THE AIR FORCE

Air Force Institute of Technology
ATTN: Library

Air Force Systems Command
ATTN: DLWM

Assistant Chief of Staff
Intelligence
Department of the Air Force
ATTN: IN

DEPARTMENT OF THE AIR FORCE (Continued)

Air Force Weapons Laboratory
Air Force Systems Command
ATTN: NTE, M. Plamondon
ATTN: NTES-S
ATTN: NT, D. Payton
ATTN: DED-A
ATTN: DED-I
ATTN: SUL
ATTN: NTES-G
ATTN: DEY
ATTN: NTEO

Research, Development & Logistics
Department of the Air Force
ATTN: SAFALR/DEP for Strat. & Space Sys.

Ballistic Missile Office
Air Force Systems Command
ATTN: MNNXH, D. Gage
ATTN: MNNX, W. Crabtree

Research, Development & Acq.
Department of the Air Force
ATTN: AFRD-M, L. Montulli
ATTN: AFRDQSM
ATTN: AFRDPN
ATTN: AFRDQA

Strategic Air Command
Department of the Air Force
ATTN: XPFS
ATTN: NRI-STINFO Library

Vela Seismological Center
ATTN: G. Ullrich

OTHER GOVERNMENT AGENCY

Federal Emergency Management Agency
ATTN: Hazard Eval. & Vul. Red. Div., G. Sisson

DEPARTMENT OF ENERGY CONTRACTORS

Lawrence Livermore Laboratory
ATTN: Document Control for D. Glenn

Los Alamos Scientific Laboratory
ATTN: Document Control for R. Sanford
ATTN: Document Control for C. Keller

Sandia Laboratories
ATTN: Document Control for Org 1250, W. Brown
ATTN: Document Control for A. Chabai

DEPARTMENT OF DEFENSE CONTRACTORS

Acurex Corp.
ATTN: C. Wolf
ATTN: J. Stockton
ATTN: K. Triebes

Aerospace Corp.
ATTN: Technical Information Services
ATTN: H. Mirels

Agbabian Associates
ATTN: M. Agbabian

DEPARTMENT OF DEFENSE CONTRACTORS (Continued)

Applied Theory, Inc.
2 cy ATTN: J. Trulio

Boeing Co.
ATTN: S. Strack
ATTN: Aerospace Library

California Research & Technology, Inc.
ATTN: Library
ATTN: M. Rosenblatt

Civil Systems, Inc.
ATTN: J. Bratton

Civil Systems, Inc.
ATTN: S. Melzer

Eric H. Wang
Civil Engineering Rsch. Fac.
ATTN: P. Lodde
ATTN: J. Kovarna

General Electric Company-TEMPO
ATTN: DASIAC

H-Tech Labs., Inc.
ATTN: B. Hartenbaum

Higgins, Auld & Associates
ATTN: N. Higgins
ATTN: H. Auld

IIT Research Institute
ATTN: Documents Library

J.H. Wiggins Co., Inc.
ATTN: J. Collins

Merritt CASES, Inc.
ATTN: Library

Nathan M. Newmark Consult. Eng. Svcs.
ATTN: N. Newmark
ATTN: W. Hall

Pacific-Sierra Research Corp..
ATTN: H. Brode

Mission Research Corp.
ATTN: C. Longmire
ATTN: G. McCartor

Pacifica Technology
ATTN: Library
ATTN: R. Allen

Physics International Co.
ATTN: J. Thomsen
ATTN: Technical Library
ATTN: F. Sauer

Science Applications, Inc.
ATTN: Technical Library
ATTN: R. Schlaug
ATTN: H. Wilson

DEPARTMENT OF DEFENSE CONTRACTORS (Continued)

R & D Associates
ATTN: R. Port
ATTN: Technical Information Center
ATTN: C. MacDonald
ATTN: J. Lewis
ATTN: J. Carpenter

Science Applications, Inc.
ATTN: D. Hove
ATTN: J. Craig

Science Applications, Inc.
ATTN: B. Chambers III

SRI International
ATTN: G. Abrahamson
ATTN: Library
ATTN: J. Colton

Systems, Science & Software
ATTN: C. Needham

Systems, Science & Software, Inc.
ATTN: Library
ATTN: K. Pyatt
ATTN: C. Dismukes
ATTN: J. Barthel

DEPARTMENT OF DEFENSE CONTRACTORS (Continued)

Systems, Science & Software, Inc.
ATTN: J. Murphy

Systems, Science & Software, Inc.
ATTN: C. Hastings

Terra Tek, Inc.
ATTN: A. Abou-Sayed
ATTN: Library

TRW Defense & Space Sys. Group
ATTN: N. Lipner
ATTN: Technical Information Center

TRW Defense & Space Sys. Group
ATTN: G. Hulcher

Weidlinger Assoc.
Consulting Engineers
ATTN: I. Sandler

Weidlinger Assoc.
Consulting Engineers
ATTN: J. Isenberg